HOKKAIDO UNIVERSITY

Title	A motion-compensated image filter for low-dose fluoroscopy in a real-time tumor-tracking radiotherapy system
Author(s)	Miyamoto, Naoki; Ishikawa, Masayori; Sutherland, Kenneth; Suzuki, Ryusuke; Matsuura, Taeko; Toramatsu, Chie; Takao, Seishin; Nihongi, Hideaki; Shimizu, Shinichi; Umegaki, Kikuo; Shirato, Hiroki
Citation	Journal Of Radiation Research, 56(1), 186-196 https://doi.org/10.1093/jrr/rru069
Issue Date	2015-01
Doc URL	http://hdl.handle.net/2115/58563
Rights(URL)	http://creativecommons.org/licenses/by-nc/4.0/
Type	article
File Information	J Radiat Res_56(1)_186-196.pdf

Instructions for use

Hokkaido University Collection of Scholarly and Academic Papers : HUSCAP

Journal of Radiation Research, 2015, 56, 186–196
doi: 10.1093/jrr/rru069 Advance Access Publication 16 August 2014

A motion-compensated image filter for low-dose fluoroscopy in a real-time tumor-tracking radiotherapy system

Naoki MIYAMOTO[1], Masayori ISHIKAWA[1,*], Kenneth SUTHERLAND[1], Ryusuke SUZUKI[2], Taeko MATSUURA[1], Chie TORAMATSU[2], Seishin TAKAO[1], Hideaki NIHONGI[1], Shinichi SHIMIZU[3], Kikuo UMEGAKI[4] and Hiroki SHIRATO[3]

[1]Department of Medical Physics, Graduate School of Medicine, Hokkaido University, North-15 West-7, Kita-ku, Sapporo 060-8638, Japan
[2]Department of Medical Physics, Hokkaido University Hospital, North-14 West-5, Kita-ku, Sapporo 060-8648, Japan
[3]Department of Radiology, Graduate School of Medicine, Hokkaido University, North-15 West-7, Kita-ku, Sapporo 060-8638, Japan
[4]Division of Quantum Science and Engineering, Graduate School of Engineering, Hokkaido University, North-15 West-7, Kita-ku, Sapporo 060-8638, Japan
*Corresponding author. Department of Medical Physics, Graduate School of Medicine, Hokkaido University, North-15 West-7, Kita-ku, Sapporo 060-8638, Japan. Tel: +81-11-706-7638; Fax: +81-11-706-7639; Email: masayori@med.hokudai.ac.jp

(Received 7 November 2013; revised 14 July 2014; accepted 14 July 2014)

In the real-time tumor-tracking radiotherapy system, a surrogate fiducial marker inserted in or near the tumor is detected by fluoroscopy to realize respiratory-gated radiotherapy. The imaging dose caused by fluoroscopy should be minimized. In this work, an image processing technique is proposed for tracing a moving marker in low-dose imaging. The proposed tracking technique is a combination of a motion-compensated recursive filter and template pattern matching. The proposed image filter can reduce motion artifacts resulting from the recursive process based on the determination of the region of interest for the next frame according to the current marker position in the fluoroscopic images. The effectiveness of the proposed technique and the expected clinical benefit were examined by phantom experimental studies with actual tumor trajectories generated from clinical patient data. It was demonstrated that the marker motion could be traced in low-dose imaging by applying the proposed algorithm with acceptable registration error and high pattern recognition score in all trajectories, although some trajectories were not able to be tracked with the conventional spatial filters or without image filters. The positional accuracy is expected to be kept within ±2 mm. The total computation time required to determine the marker position is a few milliseconds. The proposed image processing technique is applicable for imaging dose reduction.

Keywords: respiratory-gated radiotherapy; real-time tracking; respiratory motion; image processing; motion compensation; imaging dose

INTRODUCTION

The real-time tumor-tracking radiotherapy (RTRT) system was developed in order to compensate for respiratory-induced motion of tumors [1]. In the RTRT system, the 3D location of a fiducial marker inserted in or near the tumor is calculated from the projected position in a pair of fluoroscopic images obtained from two different oblique angle views of a patient. The marker is searched in the region of interest (ROI), defined as the search area, illustrated in Fig. 1a. The location with the maximum pattern recognition score (PRS), derived from the template pattern matching, is determined to be the marker position. With high X-ray tube voltage, large current and long pulse duration, recognition of the marker is relatively easy because a high PRS can be obtained at the marker location, as illustrated in Fig. 1b. However, the radiation dose due to X-ray fluoroscopy also increases. The imaging dose should be minimized [2]. The imaging dose can be naturally reduced by decreasing the X-ray tube parameters. However, the PRS at the marker location is decreased

© The Author 2014. Published by Oxford University Press on behalf of The Japan Radiation Research Society and Japanese Society for Radiation Oncology. This is an Open Access article distributed under the terms of the Creative Commons Attribution Non-Commercial License (http://creativecommons.org/licenses/by-nc/4.0/), which permits non-commercial re-use, distribution, and reproduction in any medium, provided the original work is properly cited. For commercial re-use, please contact journals.permissions@oup.com

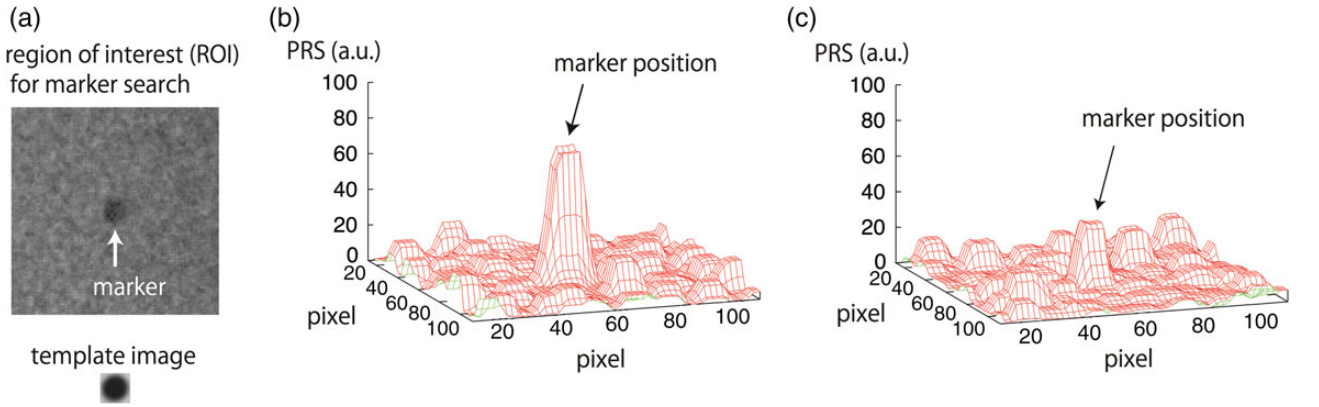

Fig. 1. (**a**) Examples of the region of interest (ROI) for the marker search and the template image. 2D distributions of the pattern recognition score (PRS) in the ROI with (**b**) high-dose imaging and (**c**) low-dose imaging.

in low-dose imaging, as indicated in Fig. 1c, as a result of image contrast degradation and the effect of statistical noise. In the case that the PRS at the marker location is low or the same as that of a neighboring region, the frequency of misidentification of the marker could be increased in template pattern matching.

One approach to improving the stability of marker tracking in low-dose imaging is the use of image filters (which can reduce the effect of statistical noise) before template pattern matching. It has been reported that an image filter is able to improve the contrast-to-noise ratio in the field of image diagnostics [3–4]. Several studies have reported that spatial filters or temporal filters are useful for removing statistical noise in low-dose fluoroscopic images [5–10]. These techniques are mainly aimed at improving the visibility of structures (such as the heart or catheters) in the fluoroscopic images. In particular, temporal filtering techniques, such as the recursive averaging filter [11], have a relatively high ability to restore the target image and to eliminate noise compared with conventional spatial filters for motionless objects, since they accumulate image signals. However, one of the limitations of using temporal filters is the generation of motion artifacts (resulting from the incorporation of information from past images).

In this study, we propose a motion-compensated recursive averaging image filter. The effectiveness of the proposed image filter was validated with a phantom experimental study utilizing respiratory motion trajectories gathered in clinical practice. The image registration error and the PRS were examined by tracking a gold spherical marker with and without the proposed image filter. Characteristics of the spatial resolution were analyzed. In order to compare the effectiveness with spatial filters (which have no motion artifact), a median filter and a smoothing filter were examined using the same technique. In addition, the feasibility of the proposed algorithm in an actual clinical scenario was validated by tracking a moving marker in the fluoroscopic images of an anthropomorphic chest phantom.

MATERIALS AND METHODS

Template pattern matching

In the RTRT system, the marker position in the fluoroscopic image is determined by means of a template pattern matching technique. The fluoroscopic image of the fiducial marker (captured before insertion into the patient) is used as the template image. Template pattern matching is based on normalized cross correlation. The correlation coefficient is given by

$$r = \frac{N\sum_{i=1}^{N} I_i M_i - \left(\sum_{i=1}^{N} I_i\right)\sum_{i=1}^{N} M_i}{\sqrt{\left|N\sum_{i=1}^{N} I_i^2 - \left(\sum_{i=1}^{N} I_i\right)^2\right|\left|N\sum_{i=1}^{N} M_i^2 - \left(\sum_{i=1}^{N} M_i\right)^2\right|}}, \quad (1)$$

where N is the pixel number, and I_i and M_i are the pixel values of the target image and the template image, respectively. The target image has to be cropped from the fluoroscopic image with the same size of the template image. The PRS is defined as

$$\mathrm{PRS} = \begin{cases} 0, & r < 0 \\ 100 \times r^2, & r \geq 0 \end{cases}. \quad (2)$$

In our case, we are not interested in the negative value, so the results are clipped to 0. The location that gives the highest PRS is considered to be the marker position in the search area. The PRS will be decreased in low-dose imaging because the image quality is degraded. By applying the image filter before the template pattern matching, the PRS could be increased in low-dose imaging. The proposed image filter is described in the following section.

Motion-compensated recursive image filter

In the recursive image averaging process, the n-th image in the image processing is expressed by

$$S_n = \alpha I_n + (1 - \alpha) S_{n-1}, \quad (3)$$

where α ($0 < \alpha < 1$) is a weight factor of the recursive process, S_n is the pixel intensity distribution of the processed image to be used for determination of the marker location by means of template pattern matching, I_n is the n-th image of the ROI in the latest fluoroscopic image, and S_{n-1} is the previously processed image. S_n is treated as S_{n-1} in the next process. In this way, the image is smoothed in time. A high degree of filtering with small α gives the maximum noise elimination power that will effectively increase the PRS, although motion artifacts of the moving object will be increased. The fiducial marker could be lost due to motion artifacts.

In order to suppress motion artifacts, a motion-compensated recursive image filter is proposed. The concept is illustrated in Fig. 2. The ROI for image processing is defined according to the current recognized position of the fiducial marker in the fluoroscopic image. As illustrated in Fig. 2, the recognized position at time t_1 is used as the center of the ROI for the next frame at t_2. In this way, the position of the fiducial marker will be located at the same relative position in the ROI when the marker moves at constant speed in the fluoroscopic image. As a result, motion artifacts of the marker can be reduced.

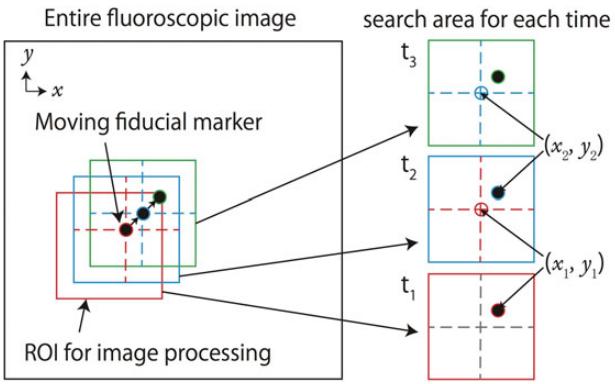

Fig. 2. Schematic diagram of motion-compensated ROI determination with the recursive filter. Black circles represent the marker position in the search area for each sequential image. Circles shown in the center of each search area represent the recognized marker positions in the previous frame.

Sample images of a moving marker tracked without image processing, with a recursive filter applied to a fixed area, and with a motion-compensated recursive filter are shown in Fig. 3a, 3b and 3c, respectively. These were the snapshots obtained by the chest phantom experiment (described later). The marker was observed on a noisy background image in the original unprocessed image seen in Fig. 3a. In the case that the recursive filter is applied with a fixed ROI, the image noise is eliminated; however, the structure of the marker is deformed, as illustrated in Fig. 3b. The marker structure was preserved by applying the proposed image filter illustrated in Fig. 3c.

The recursive filter includes the residual image of the marker, even when the marker deviates from the ROI for a reason such as a patient coughing. This residual image of the marker may be recognized by mistake. For safety, in respiratory-gated radiotherapy, irradiation of the therapeutic beam should be prohibited immediately if the marker is lost. Hence, the number of the frames in which the marker is recognized by the residual image should be minimized. The optimal weight factor (α) for our experimental set-up is investigated in this study.

Experiments

The experiments were conducted in order to investigate the optimal weight factor and to verify the effectiveness of the proposed image filter. Spatial resolution analysis and validation with a chest phantom were also conducted in the same imaging geometry. The experimental set-up is illustrated in Fig. 4. The distance between the X-ray source and the X-ray image intensifier (Color I.I., Toshiba, Japan) was fixed at 3.6 m. The image intensifier had an input surface of 23 cm diameter and was coupled to a 1000×1000 pixel resolution CCD camera (IPX-1M48, IMPERX, USA). The image depth was 8 bit. A 1.5-mm gold sphere was used as a fiducial

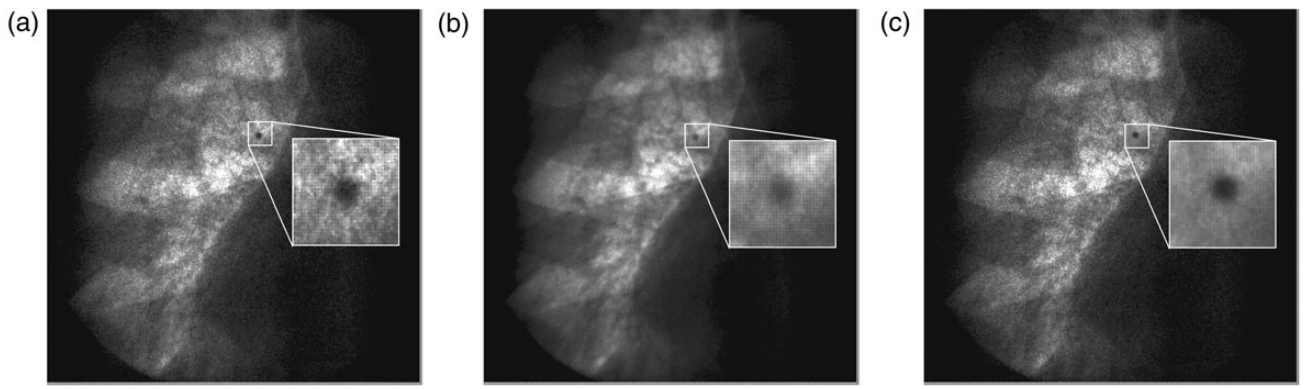

Fig. 3. Snapshot of the tracked marker (**a**) without the image processing, (**b**) with the recursive filter in fixed ROI and (**c**) with the motion-compensated recursive filter.

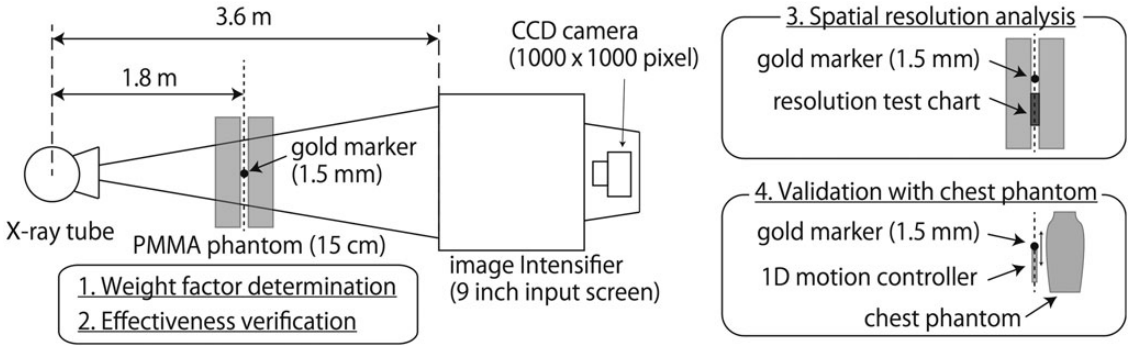

Fig. 4. Experimental set-up to gather the fluoroscopic images.

marker. In the RTRT system, 3D location of the internal marker is calculated from two projected marker locations obtained by means of two fluoroscopy systems with the same specs. Hence, validation with the single imaging system is enough to evaluate the effectiveness of the proposed image filter. The details for each evaluation are described in the following sections.

Determination of weight factor

The fiducial marker was sandwiched between polymethylmethacrylate (PMMA) slabs. A PMMA thickness of 150 mm was assumed to be approximately equal to the imaging condition of chest fluoroscopy. About 450 fluoroscopic images of the static marker were recorded at a frame rate of 30 images per second. This frame number was assumed to be sufficient for evaluating the statistics of marker tracking. Template pattern matching was conducted in the fixed search area ROI_a including the marker, as shown in Fig. 7a, from the first image in the sequence. Then, the search area was changed to ROI_b, which did not include the marker. The average and SD of the pixel value in each region, ROI_a and ROI_b, were equivalent. In this way, the deviation or loss of the marker from the ROI was simulated. Time-series data of the PRS were investigated in order to evaluate the effect of the residual image of the marker. Four weight factors were applied: $\alpha = 0.125$, 0.25, 0.5 and 0.75. Template pattern matching and the recursive filter were performed with a commercially available software tool (Matrox Imaging Library 9.0, Matrox Electronic Systems Ltd, Canada). The size of the template image and the ROI for marker search were 18×18 pixels and 64×64 pixels, respectively.

The tube voltage and exposure duration were fixed at 58 kV and 2.5 ms, respectively. The minimum tube current for recognizing the marker without an image filter was confirmed to be 50 mA by monitoring the registration position of the static marker during fluoroscopy. Hence, a tube current of 50 mA was considered to be low-dose imaging in this setup. For clinical use, optimization algorithms of the fluoroscopy parameters [12–13] could be useful in order to find low-dose imaging conditions.

Effectiveness verification of image filter

The same images used for the weighting factor determination were also used for the effectiveness evaluation of the proposed image filter. The main purpose of the evaluation was to evaluate the tracking stability and the registration error caused by motion artifacts rather than any anatomical structure. Hence, the images of PMMA slabs were sufficient for evaluation. In order to determine the marker registration accuracy quantitatively and with actual tumor motion, the images were shifted sequentially in order to mimic the motion of the marker shadow on the fluoroscopic image caused by respiration. 3D trajectory data of the fiducial marker, gathered by the RTRT system in clinical practice, were used in order to reproduce the motion of the marker shadow. A total of 383 trajectories from 76 patients were used. Each patient provided between one and 10 trajectories. The breathing cycle that was derived from the power spectrum of the Fourier transform signal in the CC direction was 3.4 ± 0.8 s. The numbers of trajectories that had motion >10 mm, 5–10 mm and <5 mm were 114, 181 and 88 cases, respectively. The absolute registration error and the PRS were examined for each trajectory. The registration error was defined as the 2D discrepancy between the actual marker position and the recognized marker position in the fluoroscopic image. Template pattern matching was conducted with subpixel accuracy. The ROI size for the marker search area was 64×64 pixels, and the search area for the next process was shifted sequentially according to the current recognized position.

The trajectories include measurement error because of fluctuations in the marker recognition and/or misidentification of the marker, as illustrated in Fig. 5a. In order to eliminate the measurement uncertainties and to extract the marker motion itself, two types of noise filters were applied to the original raw trajectory data. First, a median filter with window size of ~165 ms, corresponding to five frames, was applied to eliminate spike noise caused from misidentification of the marker. Second, a low-pass filter based on the Fourier transform was applied to eliminate random error. A cut-off frequency of 5 Hz was applied in order to preserve the physical motion, including breathing and heartbeat. The

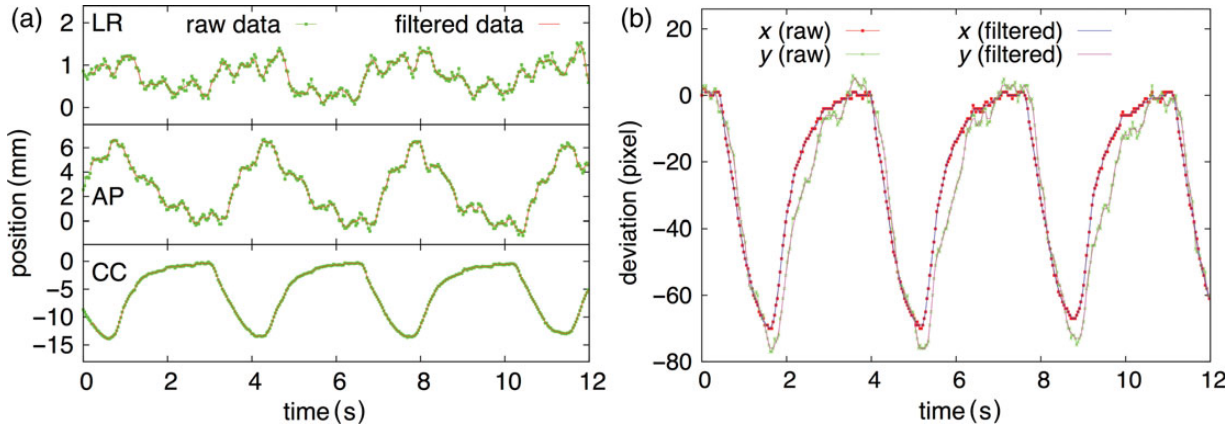

Fig. 5. (**a**) Example of the raw trajectory data gathered by the RTRT system and the filtered data for LR, AP and CC directions. (**b**) Deviation of the 2D projected marker position in the fluoroscopic image.

time-series data of the filtered 3D trajectory shown in Fig. 5a was then converted to the projected position, which was rounded to an integer value in the fluoroscopic image by assuming the imaging geometry of the RTRT system to be as shown in Fig. 5b.

In order to distinguish the success or failure of tracking, the pass-rate was defined as the ratio of the number of frames within a registration error of 10 pixels to the number of all processed frames. The registration error of 10 pixels in the fluoroscopic image induces a 3D measurement error of ~1 mm at most. A pass-rate of >95% was considered to be successful. In the motion-compensated recursive filter, the pass-rate may depend on the starting position of tracking in the respiratory motion, because conformation of an averaged image in the first few frames depends on the speed of the marker. For instance, for respiration-induced tumor motion, the duration of exhalation is usually longer than that of inhalation. In order to estimate the effect of the starting point, tracking was started from three respiratory phases: exhalation, middle and inhalation.

For comparison with spatial filters that have no motion artifact, a median filter and a smoothing filter were examined in the same way. The window size for deriving the median pixel value was 3×3 pixels. In the smoothing filter, a 3×3 kernel was utilized, with the center pixel contributing one-quarter of its value to the result, each of the four pixels above, below, left and right of the center contributing one-eighth, and the others contributing 1/16. In the same way, the position of the search area for the marker search was shifted according to the recognized marker position.

The marker motion during X-ray exposure was not considered in this analysis, because the static marker was taken in all sequential images. The maximum speed of the marker was ~22.2 mm/s in all trajectories. The movement of the marker during the exposure was ~0.06 mm when the pulse duration and the marker speed were 2.5 ms and 22.2 mm/s, respectively. This movement of the marker is relatively small compared with the marker diameter of 1.5 mm. Hence, it was assumed that the effect of motion blur caused by marker motion during the exposure can be ignored in this study.

Spatial resolution analysis

In the proposed image filter, the spatial resolution of the image should be changed according to the variation in the marker speed [14]. The registration error of the fiducial marker could depend on the spatial resolution. The spatial resolution and the registration error in the proposed image filter were evaluated in the best and the worst scenarios. The images of the fiducial marker and the resolution test chart placed beside the marker were acquired in the same geometry as that shown in Fig. 4. In order to reproduce respiratory motion, the acquired images were shifted sequentially with the trajectory that contained maximum variation in marker speed. Spatial resolution and the registration error were examined by analyzing the images that were captured at the minimum and the maximum variations in marker speed and considered the 'best' and the 'worst' cases, respectively. The tube voltage, current and exposure duration were 70 kV, 50 mA and 2.5 ms, respectively. In this evaluation, the tube voltage was increased from that of the previous experiments in order to improve the visibility of the resolution test chart.

Validation with chest phantom image

In the previous evaluations, the effectiveness was validated with the homogeneous phantom, although actual clinical images are associated with a range of thicknesses. In order to confirm that the proposed technique for tracking the marker in inhomogeneous images (i.e. those involving a large variation in contrast and/or thickness), an experiment using an anthropomorphic chest phantom (LUNGMAN, Kyoto Kagaku Co. Ltd, Japan) was performed. The alignment of the X-ray tube and the XRII was the same as in the previous experiment. The gold marker was placed in front of the chest phantom and was moved using the 1D motion controller, as shown in Fig. 4. The motion controller mimicked periodical marker motion.

The marker was moved perpendicular to the imaging axis with a maximum speed of ~20 mm/s in order to simulate the maximum speed and acceleration observed in actual clinical cases. An example of a fluoroscopic image is shown in Fig. 6. The white arrow indicates the marker trajectory in the fluoroscopic image. In the fluoroscopic images obtained, the marker moved within a region of varying media, which included the lung, bone and heart. Region A, illustrated in Fig. 6, was a thin region comprised mainly of the lung. Region B was a thicker region compared with Region A, and included the heart and bone. The tube voltage and exposure duration were fixed at 50 kV and 2.5 ms, respectively. Tube currents of 50 mA and 100 mA were examined. The PRS with and without the image filter was evaluated.

RESULTS

Determination of weight factor

The time-series data of the PRS obtained by tracking the stable marker for each weight factor is illustrated in Fig. 7b.

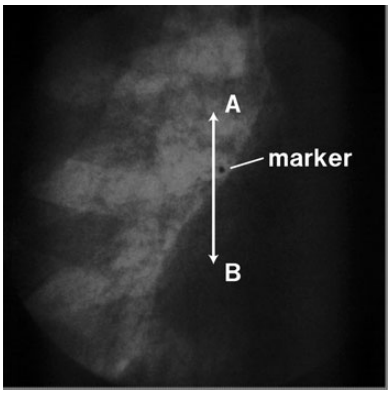

Fig. 6. Example of an X-ray fluoroscopic image of the chest phantom and the marker. The marker was moved sinusoidally between A and B.

The PRS was improved as the degree of recursive filter was increased, as indicated by the result of ROI_a. In addition, the fluctuation of the PRS was decreased similarly. The search area was changed from ROI_a to ROI_b at frame number 100. The PRS dropped immediately after the ROI shift. However, the PRS obtained with $\alpha = 0.125$ and 0.25 at the time of the ROI shift was high compared with that of other degrees, although the marker was not included in the search area. This was caused by the residual image of the marker. The degree of the recursive filter should be reduced if the residual image is retained for several frames, as shown in the result obtained with $\alpha = 0.125$. In the case of $\alpha = 0.25$, the recognition of the residual image can be avoided by applying an appropriate threshold PRS. Hence, the optimal weight factor was determined to be 0.25 in our experimental set-up.

Effectiveness verification of image filter

The number of the trajectories regarded as successful and the statistical details of the pass-rate for each image filter are summarized in Table 1. The proposed image filter, when the starting point was at exhalation, was able to track the marker successfully in all tested trajectories. For other starting points, it also worked successfully, except for in one case. Hence, the effect of the starting position was thought to be unimportant with an image acquisition rate of 30 frames per second. On the other hand, failures of tracking were often observed with other spatial filters.

An example of the recognized position of the trajectory being regarded as successful with all image filters is shown in Fig. 8a. The results, except for the proposed image filter, included temporary misidentification, shown as spikes in the graph. If such unstable registration is continued for several frames, the marker will be lost, as illustrated in Fig. 8b, since the search area is not properly updated. The registration error and the PRS corresponding to the data of Fig. 8a are shown in Fig. 8c and 8d, respectively. There was no misidentification in

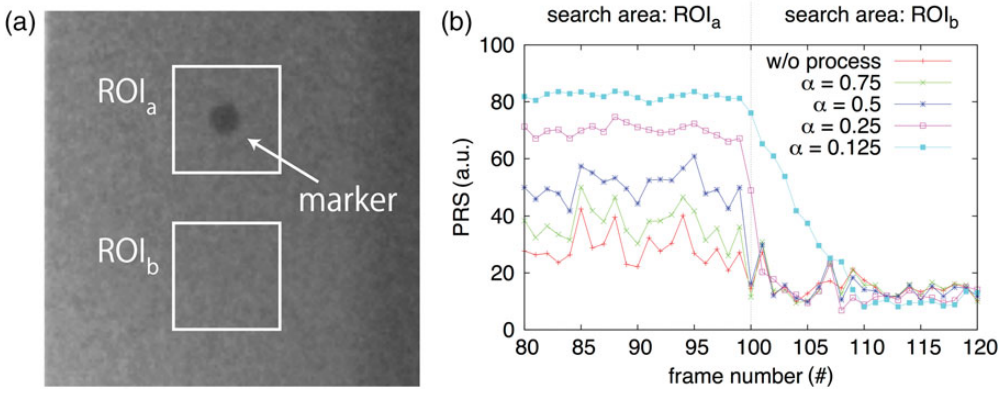

Fig. 7. (**a**) Example of a fluoroscopic image and the location of ROI_a and ROI_b. (**b**) Time-series data of the PRS for each weight factor.

Table 1. Number of trajectories for which the pass-rate was over 95 out of 383 trajectories and statistical details of the pass-rate in the group of successful cases for each image filter: motion-compensated recursive image filter for which starting point is the (1) exhalation, (2) middle and (3) inhalation respiratory phases; (4) median filter, (5) smoothing filter and (6) without image filter.

Image filter	Number of trajectories in successful cases (%)	Pass-rate of success			
		mean	SD	min.	max.
(1) Recursive/ exhalation	383 (100.0)	100.0	0.1	99.3	100.0
(2) Recursive/ middle	382 (99.7)	100.0	0.1	98.7	100.0
(3) Recursive/ inhalation	382 (99.7)	100.0	0.1	98.5	100.0
(4) Median	299 (78.1)	96.0	0.4	95.2	97.2
(5) Smoothing	230 (60.1)	96.0	0.4	95.2	97.2
(6) W/o filter	339 (88.5)	97.3	0.4	95.2	98.3

the proposed image filter during tracking. In addition, the highest PRS was obtained with the proposed image filter. The statistical details of the registration error and the PRS in the trajectories for each image filter are summarized in Table 2. The mean, SD and maximum registration error for the proposed filter were the lowest. Also, the mean PRS was the highest and the SD of the PRS was the lowest. The minimum value of the PRS for the proposed filter was observed around the first frame because the initial recognition must be applied to an unprocessed image. Hence, the initial recognition may be unstable due to lower dose imaging. Additional processes may be implemented in order to avoid instability of the initial recognition. First, the tracking can be started with high-dose imaging without image filter. The X-ray tube parameter can then be reduced gradually and the image filter applied. In this way, instability of the initial recognition and the failure due to the starting point of the tracking can be avoided.

In the case that the size of the search area and the template image were 64×64 and 18×18 pixels, respectively, the time to calculate the PRS was within 1 ms using a commercially

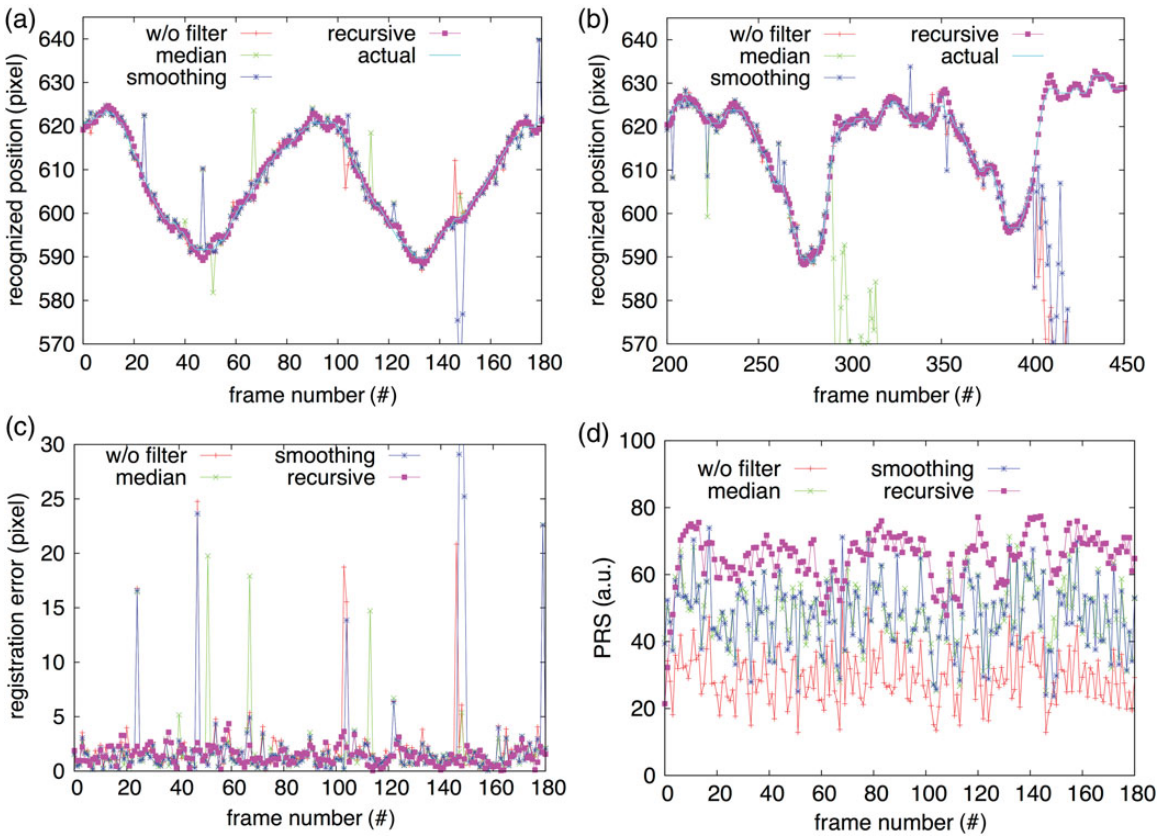

Fig. 8. Examples of time-series data: (**a**) recognized position of the trajectory regarded as successful of tracking with all image filters, (**b**) recognized position of the trajectory regarded as failure of tracking with image filters except for the proposed image filter, (**c**) registration error, (**d**) PRS.

Table 2. Statistics of the registration error and the pattern recognition score (PRS) in the marker tracking for each image filter: motion-compensated recursive image filter for which the starting point is the (1) exhalation, (2) middle and (3) inhalation respiratory phases; (4) median filter, (5) smoothing filter, and (6) without image filter

Image filter		Registration error (pixel)				PRS (a.u.)			
	n	mean	SD	min.	max.	mean	SD	min.	max.
(1) Recursive/exhalation	383	1.4	0.9	0.0	18.5	64.0	7.2	18.4	81.2
(2) Recursive/middle	382	1.4	0.9	0.0	30.6	64.0	7.2	15.4	81.4
(3) Recursive/inhalation	382	1.4	0.9	0.0	17.3	64.0	7.2	16.4	81.2
(4) Median	299	2.3	4.9	0.0	58.6	48.5	10.4	19.7	73.9
(5) Smoothing	230	2.6	5.9	0.0	51.6	47.9	10.5	21.1	73.9
(6) W/o filter	339	2.1	3.9	0.0	57.7	29.1	7.8	7.3	51.8

n = the number of successful cases. Tube current, voltage and pulse duration were 50 mA, 58 kV and 2.5 ms, respectively.

available PC (Intel Core2 Quad CPU, 2.40 GHz) and software tool (Matrox Imaging Library 9.0, Matrox Electronic Systems Ltd, Canada). The time for the motion-compensated recursive filter was also less than 1 ms. Hence, the total computation time for the proposed algorithm to determine the marker location will be within a few milliseconds.

Spatial resolution analysis

The images of the marker and the resolution test chart obtained without the image filter, with the image filter at the minimum and the maximum variations in marker speed are shown in Fig. 9a, 9b and 9c, respectively. Random image noise shown in Fig. 9a was reduced by applying the proposed image filter, as shown in Fig. 9b and 9c. However, motion blur was large in Fig. 9c due to large variation in marker speed, which was a result of both acceleration and deceleration. In order to evaluate the spatial resolution, the profiles along the dashed lines drawn in the images are shown in Fig. 9d, 9e and 9f. For comparison, the results of the median filter and the smoothing filter are added to Fig. 9d. The stripes of 1.0 lp/mm were not clearly shown in Fig. 9d because of low contrast noise ratio. In the best performance of the proposed image filter, the stripes of 1.0 lp/mm were preserved, as shown in Fig. 9e. In the worst case, illustrated in Fig. 9f, spatial resolution was degraded and the marker image had motion blur.

The registration error of the marker in the best and the worst cases of the proposed image filter were 0.4 and 8.1 pixels, respectively. The registration errors without image filter, median filter and smoothing filter were 0.7, 0.6 and 0.7 pixels, respectively. It was thought that better registration accuracy was obtained with better spatial resolution.

Validation with chest phantom image

The recognized positions and the PRS of the moving marker in the tube current of 50 mA are shown in Fig. 10a and 10b, respectively. The results with the tube current of 100 mA are shown in Fig. 10c and 10d, respectively. The PRS was decreased in Region B due to the low image contrast of the thick region in both sets of imaging conditions: 50 mA and 100 mA. In Fig. 10a, the marker tracking without the image filter failed around Region B. Correspondingly, the lower PRS was obtained as shown in Fig. 10b. The primary causes of PRS degradation are assumed to be effect of statistical noise, low contrast of the image, and the structure of the background image. Mean ± SD, and maximum and minimum of PRS for 100 mA without the image filter were 58.2 ± 23.9, 91.4 and 11.2, respectively. On the other hand, the marker was traced correctly in both tube current settings by applying the image filter. The PRS was improved in all regions that had various thicknesses, including anatomical contrast. Mean ± SD, maximum and minimum of PRS for 100 mA with the image filter were 69.9 ± 20.4, 94.3 and 42.0, respectively. It is thought that the noise and structures will be removed or smoothed by image averaging in the proposed image filter. The marker was tracked correctly by applying the proposed image filter, while the marker was lost in the case without the image filter.

DISCUSSION

In order to estimate the clinical benefit, the expected improvement of the tracking stability and dose reduction using the motion-compensated recursive image filter are discussed. The PRS and the registration error were examined in a similar way for 383 trajectories in five cases: (1) tube current of 50 mA with the motion-compensated recursive filter as low-dose imaging, (2, 3) tube current of 80 mA with and without the filter as middle-dose imaging, (4, 5) tube current of 100 mA with and without the filter as high-dose imaging. Tube voltage and exposure duration were fixed at 58 kV and 2.5 ms, respectively. The statistics of the registration error and the PRS are summarized in Table 3. The PRS in low-dose imaging with the image filter was higher than that of middle- and high-dose imaging without the image filter.

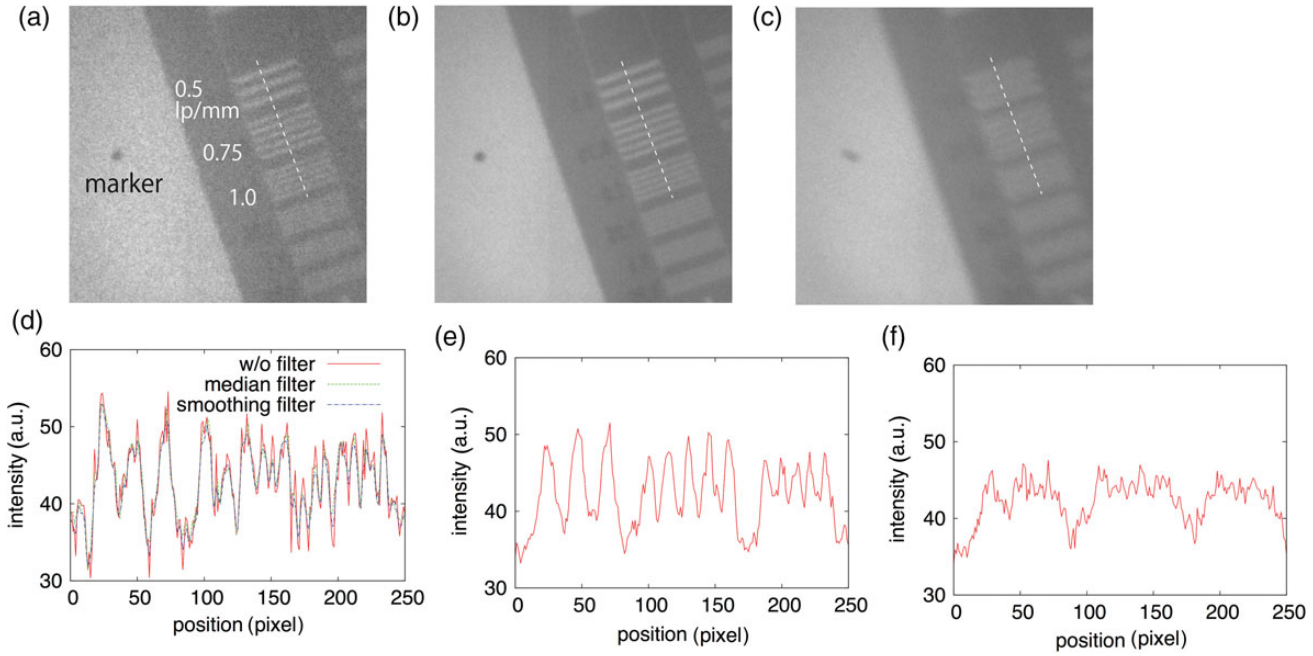

Fig. 9. (**a**) X-ray image of the marker and the resolution test chart without image filter, (**b**) with motion-compensated image filter at the minimum variation in marker speed and (**c**) the maximum variation in marker speed. Corresponding profiles along the dashed line are shown in (d), (e) and (f).

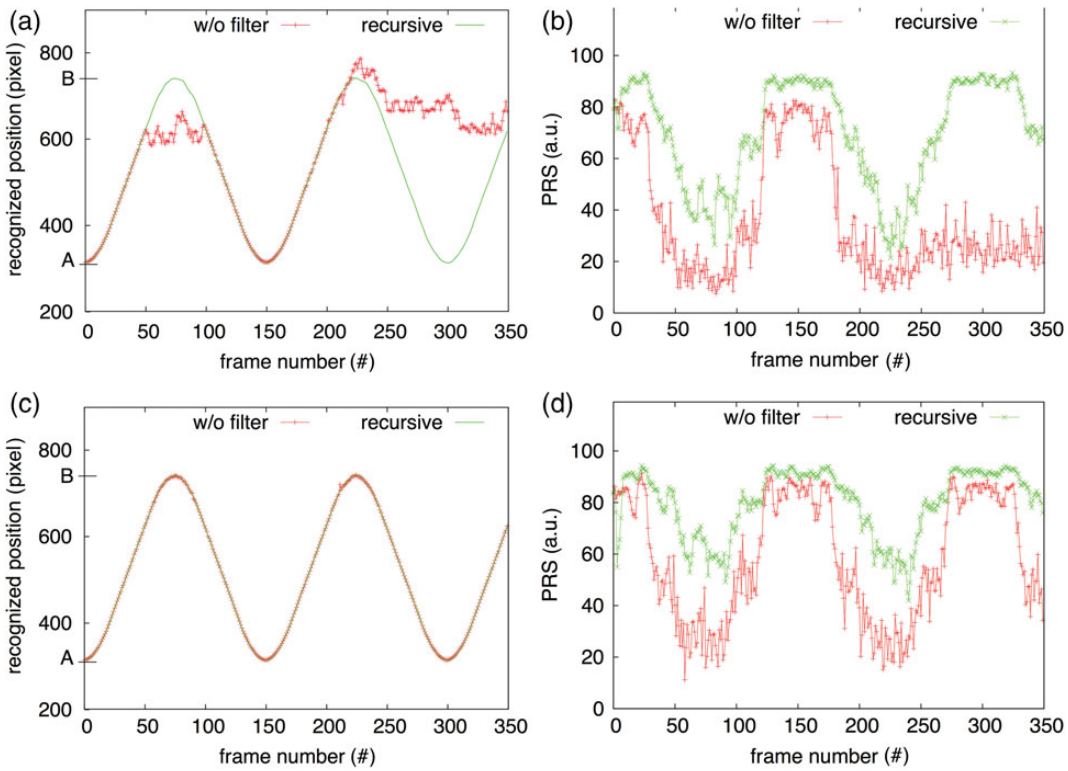

Fig. 10. Time-series data: (**a**) recognized positions and (**b**) PRS in the tube current of 50 mA; (**c**) recognized positions and (**d**) PRS in the tube current of 100 mA. The marker tracking without the image filter failed around Region B in low-dose imaging. Correspondingly, the lower PRS was observed. The marker was traced correctly in both tube current settings by applying the image filter. Also, the PRS was improved.

The registration error of low-dose imaging was acceptable, although it was higher than that of middle- and high-dose imaging without the image filter. The maximum registration error due to unstable registration fluctuated regardless of imaging dose. In this evaluation, average and SD of the registration error were slightly worse in middle- and high-dose imaging with the proposed image filter compared with low-dose imaging (because of larger maximum registration error). The total positional accuracy was expected to be within the tolerance recommended (positional accuracy <2 mm) by the AAPM Task Group 142 for respiratory-gated radiation therapy [15]. The PRS was also improved in middle- and high-dose imaging by applying the image filter. Furthermore, the PRS was improved in the imaging condition that had originally high PRS, as shown in Fig. 10b and d. Hence, the proposed image filter was thought to be robust to the thickness and kiloVolt exposure parameters. These results suggest that the imaging dose could be reduced while maintaining the same tracking stability with similar accuracy to high-dose imaging. A typical treatment schedule of lung RTRT is 40 or 48 Gy for four fractions. About 30 min of fluoroscopy take for each treatment day in the current system. Assuming the typical dose rate of 300 mGy/h at the skin surface [16] with one fluoroscopy unit, the accumulated imaging dose given by two fluoroscopy units could be ~1.2 Gy. The imaging dose could be larger when high-dose imaging is need. Hence, reduction of the imaging dose is required.

There were two limitations in the proposed image filter in this work. The first one was that the ROI was able to be shifted by only integer values in the image averaging process. The second was the variation in the speed of the marker. In the proposed image filter, motion artifacts can be compensated for accurately when the marker moves at a constant speed in the fluoroscopic images. The variation in the speed affects the registration accuracy since the location of the marker in the ROI shown in Fig. 2 will be shifted slightly. In order to quantify the effect of the variation in the speed to the registration error of the marker, the deviation of the marker location in the search area between the frames in the motion-compensated ROI determination was examined for each trajectory. Mean ± SD, maximum and 95% percentile of deviation were 0.6 ± 0.5, 4.0 and 1.4 pixels, respectively, with the fluoroscopy operated at 30 frames per second. Hence, the variation in the speed of the marker should be one of the primary contributors to registration error, as shown in spatial resolution analysis. Even if the image filter is applied, the marker could be lost when the fluoroscopic parameters are too low. In normal use, fluoroscopy is stopped when the marker is lost. Fluoroscopic parameters are then adjusted again.

Reduction of the frame rate of fluoroscopy is one simple method for reducing imaging dose. However, registration errors for the proposed image filter will be increased since the variation in the marker speed between the frames is increased in fluoroscopy with a lower frame rate. For instance, the deviation of mean ± SD, maximum and 95% quantiles were 1.3 ± 1.3, 16.6 and 3.8 pixels, respectively, assuming fluoroscopy of 10 frames per second. In such a case, the prediction techniques [17–20] have the potential to compensate for this variation in marker location in motion-compensated ROI determination. Ren *et al.* showed a prediction error of ~0.5 mm (corresponding to at most 5 pixels in our study) in real time imaging of 10 Hz to compensate for the system latency [20]. It could compensate large discrepancy that leads to misidentification of the marker. Hence, further reduction of the imaging dose may be realized by applying the prediction techniques.

Table 3. Statistics of the registration error and the PRS in five imaging conditions: (1) tube current of 50 mA with the motion-compensated recursive filter as low-dose imaging, (2, 3) tube current of 80 mA with and without image filter as middle-dose imaging, and (4, 5) tube current of 100 mA with and without image filter as high-dose imaging

	Registration error (pixel)				PRS (a.u.)			
Dose/image filter	**mean**	**SD**	**min**	**max**	**mean**	**SD**	**min**	**max**
(1) Low/recursive	1.4	0.9	0.0	18.5	64.0	7.2	18.4	81.2
(2) Middle/recursive	1.6	1.1	0.0	31.2	79.2	6.6	24.2	90.7
(3) Middle/none	0.8	0.5	0.0	3.3	48.7	6.8	21.1	68.0
(4) High/recursive	1.5	1.0	0.0	20.4	83.1	5.1	27.8	91.6
(5) High/none	0.8	0.4	0.0	3.0	54.8	6.1	30.9	74.0

CONCLUSION

In this work, a motion-compensated recursive image filter was proposed in order to track a fiducial marker with acceptable registration error and with short computation time in low-dose imaging in the RTRT system. In a phantom study with actual tumor motion, the proposed image filter was able to track the marker motion with high PRS and acceptable registration error in all tested trajectories, including those that were not able to be tracked with conventional spatial filters or without image filter. The positional accuracy is expected to be kept to within 2 mm. The total computation time, a few milliseconds, including template pattern matching and image processing, is negligible compared with other system delays. In addition, it was shown that the proposed image processing technique can work to track the marker in the image quality equivalent to actual fluoroscopy. In conclusion, the proposed image processing technique, which is a combination of a motion-compensated recursive filter and template pattern matching, is applicable for low-dose fluoroscopy in the RTRT system.

FUNDING

This research was partly funded by a grant from the Japan Society for the Promotion of Science (JSPS) through the 'Funding Program for World-Leading Innovative R&D on Science and Technology (FIRST Program)' initiated by the Council for Science and Technology Policy (CSTP). The research formed part of a 'Research and Development Project on Treatment Equipment Using High Accurate X-Ray Radiation', which Hokkaido University contracted with the New Energy and Industrial Technology Development Organization (NEDO). Funding to pay the Open Access publication charges for this article was provided by NEDO.

REFERENCES

1. Shirato H, Shimizu S, Shimizu T *et al*. Real-time tumor-tracking radiotherapy. *Lancet* 1999;**353**:1331–2.
2. Murphy MJ, Balter J, Balter S *et al*. The management of imaging dose during image-guided radiotherapy: report of the AAPM task group 75. *Med Phys* 2007;**34**:4041–63.
3. Baydush AH, Floyd CEJ. Improved image quality in digital mammography with image processing. *Med Phys* 2000;**27**:1503–8.
4. Zanca F, Jacobs J, Van Ongeval C *et al*. Evaluation of clinical image processing algorithms used in digital mammography. *Med Phys* 2009;**36**:765–75.
5. Chan CL, Katsaggelos AK, Sahakian AV. Image sequence filtering in quantum-limited noise with applications to low-dose fluoroscopy. *IEEE Trans Med Imaging* 1993;**12**:610–21.
6. Wilson DL, Jabri KN, Aufrichtig R. Perception of temporally filtered X-ray fluoroscopy images. *IEEE Trans Med Imaging* 1999;**18**:22–31.
7. Jabri KN, Wilson DL. Detection improvement in spatially filtered x-ray fluoroscopy image sequences. *J Opt Soc Am A Opt Image Sci Vis* 1999;**16**:742–9.
8. Sanchez-Marin FJ, Srinivas Y, Jabri KN *et al*. Quantitative image quality analysis of a nonlinear spatio-temporal filter. *IEEE Trans Image Process* 2001;**10**:288–95.
9. Wang J, Zhu L, Xing L. Noise reduction in low-dose x-ray fluoroscopy for image-guided radiation therapy. *Int J Radiat Oncol Biol Phys* 2009;**74**:637–43.
10. Nishiki M, Shiraishi K, Sakaguchi T *et al*. Method for reducing noise in X-ray images by averaging pixels based on the normalized difference with the relevant pixel. *Radiol Phys Technol* 2008;**1**:188–95.
11. Kruger RA. A method for time domain filtering using computerized fluoroscopy. *Med Phys* 1981;**8**:466–70.
12. Tapiovaara MJ, Sandborg M, Dance DR. A search for improved technique factors in paediatric fluoroscopy. *Phys Med Biol* 1999;**44**:537–59.
13. Miyamoto N, Ishikawa M, Bengua G *et al*. Optimization of fluoroscopy parameters using pattern matching prediction in the real-time tumor-tracking radiotherapy system. *Phys Med Biol* 2011;**56**:4803–13.
14. Shirato H, Suzuki K, Sharp GC *et al*. Speed and amplitude of lung tumor motion precisely detected in four-dimensional setup and in real-time tumor-tracking radiotherapy. *Int J Radiat Oncol Biol Phys* 2006;**64**:1229–36.
15. Klein EE, Hanley J, Bayouth J *et al*. Task group 142 report: quality assurance of medical accelerators. *Med Phys* 2009; **36**:4197–212.
16. Shirato H, Oita M, Fujita K *et al*. Feasibility of synchronization of real-time tumor-tracking radiotherapy and intensity-modulated radiotherapy from viewpoint of excessive dose from fluoroscopy. *Int J Radiat Oncol Biol Phys* 2004;**60**:335–441.
17. Sharp GC, Jiang SB, Shimizu S *et al*. Prediction of respiratory tumour motion for real-time image-guided radiotherapy. *Phys Med Biol* 2004;**49**:425–40.
18. Vedam SS, Keall PJ, Docef A *et al*. Predicting respiratory motion for four-dimensional radiotherapy. *Med Phys* 2004; **31**:2274–83.
19. Ruan D, Fessler JA, Balter JM. Real-time prediction of respiratory motion based on local regression methods. *Phys Med Biol* 2007;**52**:7137–52.
20. Ren Q, Nishioka S, Shirato H *et al*. Adaptive prediction of respiratory motion for motion compensation radiotherapy. *Phys Med Biol* 2007;**52**:6651–61.